Radiological Physics and Technology (2024) 17:441–450
https://doi.org/10.1007/s12194-024-00797-8

RESEARCH ARTICLE

Evaluation of hafnium oxide nanoparticles imaging characteristics as a contrast agent in X-ray computed tomography

Arash Safari[1,2] · Maziyar Mahdavi[1,2] · Reza Fardid[1,2] · Alireza Oveisi[3] · Reza Jalli[4] · Masoud Haghani[1,2]

Received: 23 December 2023 / Revised: 18 March 2024 / Accepted: 19 March 2024 / Published online: 17 April 2024

Abstract

This research aimed to compare the quantitative imaging attributes of synthesized hafnium oxide nanoparticles (NPs) derived from UiO-66-NH2(Hf) and two gadolinium- and iodine-based clinical contrast agents (CAs) using cylindrical phantom. Aqueous solutions of the studied CAs, containing 2.5, 5, and 10 mg/mL of HfO_2NPs, gadolinium, and iodine, were prepared. Constructed within a cylindrical phantom, 15 cc small tubes were filled with CAs. Maintaining constant mAs, the phantom underwent scanning at tube voltage variations from 80 to 140 kVp. The CT numbers were quantified in Hounsfield units (HU), and the contrast-to-noise ratios (CNR) were calculated within delineated regions of interest (ROI) for all CAs. The HfO_2NPs at 140 kVp and concentration of 2.5 mg/ml exhibited 2.3- and 1.3-times higher CT numbers than iodine and gadolinium, respectively. Notably, gadolinium consistently displayed higher CT numbers than iodine across all exposure techniques and concentrations. At the highest tube potential, the maximum amount of the CAs CT numbers was attained, and at 140 kVp and concentration of 2.5 mg/ml of HfO_2NPs the CNR surpassed iodine by 114%, and gadolinium by 30%, respectively. HfO_2NPs, as a contrast agent, demonstrated superior image quality in terms of contrast and noise in comparison to iodine- and gadolinium-based contrast media, particularly at higher energies of X-ray in computed tomography. Thus, its utilization is highly recommended in CT.

Keywords HfO_2NPs · Metal–organic framework · Contrast media · X-ray computed tomography · Nanoparticle

1 Introduction

Numerous studies have explored the utilization of high atomic number (Z) nanoparticles as contrast agents (CAs) in diagnostic radiology [1]. Computed tomography (CT) is a widely employed imaging modality for diagnosing various diseases, providing detailed cross-sectional images of the body, which offers valuable anatomical information, helping correlate clinical and pathological findings and aiding in the identification of suspected lesions, their locations, sizes, and extent [2, 3]. CT imaging relies on measuring the X-ray attenuation coefficients of different tissues, which vary based on their atomic number and density. In diagnostic energy ranges, atomic number and density play a crucial role, with higher atomic number and density resulting in greater photon attenuation. This is particularly relevant to the photon energy range, where photoelectric and Compton effects dominate as the primary mechanisms of photon interaction with matter. Materials with high X-ray attenuation coefficients, such as bone, significantly absorb much more X-rays than soft tissues in the body [4, 5]. For this reason, to achieve beneficial contrast resolution in soft tissue, artificial CA with high atomic numbers and densities are used to enhance the photoelectric effect in clinical practice. The vascular structures, the urinary and gastrointestinal tract, and perfusion assessments are enhanced by these agents.

✉ Arash Safari
arash.safari1985@gmail.com

✉ Alireza Oveisi
aroveisi@uoz.ac.ir

✉ Masoud Haghani
m.haghani4744@yahoo.com

[1] Ionizing and Non-Ionizing Radiation Protection Research Center (INIRPRC), School of Paramedical Sciences, Shiraz University of Medical Sciences, Shiraz, Iran

[2] Department of Radiology, School of Paramedical Sciences, Shiraz University of Medical Sciences, Shiraz, Iran

[3] Department of Chemistry, Faculty of Sciences, University of Zabol, P.O. Box: 98615-538, Zabol, Iran

[4] Department of Radiology, Medical Imaging Research Center, Shiraz University of Medical Sciences, Shiraz, Iran

Thereby, increasing contrast in the reconstructed images of both static and dynamic CT scans could be achieved.

In many studies, heavy element CAs such as barium, bismuth, gold, gadolinium, or iodine have been used as CT contrast media [6]. Iodine-based contrast media are widely used for CT imaging due to their rapid enhancement of blood vessels and organs, versatility in different imaging techniques, affordability, and water-soluble properties and causes a short imaging time. However, these materials have some disadvantages and potential side effects, including allergic reactions, nephrotoxicity, thyroid effects, vomiting, and vascular extravasation. Patients with certain medical conditions, such as multiple myeloma or sickle cell anemia, may have an increased risk of adverse effects from iodine-based contrast media. Furthermore, the typical range of tube voltages (80 – 140 kVp), employed in modern computed tomography (CT) scanners, work well for general imaging purposes, but the inherent limitation lies in the K-edge energy of some ordinary contrast media. In the diagnostically utilized X-ray CT spectrum, iodine's contrast-enhancing capabilities are not fully exploited. Because iodine's K-edge is located at a relatively low energy level of only 33.2 keV [7–10].

Unlike iodine-based CAs, gadolinium-based CAs do not significantly interfere with laboratory tests, making them suitable for being primarily used as CA in magnetic resonance imaging (MRI). However, their metal content is too low to be used as effective (CAs) in CT. This is because CT scans require a higher metal content to produce the contrast needed for clear imaging, which gadolinium-based contrast agents cannot provide due to their low metal content [11]. Nevertheless, the most significant concerns associated with gadolinium-based CAs are the risk of developing nephrogenic systemic fibrosis, retention in the body, particularly in the brain, and their higher cost [12–15].

To overcome this limitation and improved X-ray attenuation significantly, researchers have turned to high atomic number (Z) elements, which exhibit K-edges within the range of 60 – 80 keV. The strategic selection has potentially and substantially yielded enhanced contrast in X-ray CT imaging of the elements with higher K-edge energies [16]. By optimizing the selection of contrast agents based on their K-edge energies, researchers can unlock new opportunities for better tissue visualization and improved diagnostic image quality in modern CT imaging. Hafnium (Hf), a high atomic number element ($Z = 72$), exhibits strong photon absorption at energies higher than 65 keV, making it significantly promising as a CT CA. This element boasts of impressive properties such as stretchability, high-temperature resistance, processability, and corrosion resistance [17]. Moreover, hafnium oxide nanoparticles (HfO_2NPs) possess inert characteristics and show no toxicity to living cells, rendering them promising candidates in numerous clinical trials [18, 19]. Notably, a phase II/III trial demonstrated positive outcomes for patients with soft tissue sarcomas using HfO_2NPs [20]. A novel class of highly stable hafnium and lanthanide as inositol complexes has been synthesized and thoroughly characterized, which display excellent water solubility and high suitability as CT CAs (17). These innovative hafnium complexes represent a promising new generation of X-ray CAs, and their high K-edge also suggests potential compatibility with the newly developed photon-counting CT detectors, particularly in K-edge imaging applications [21].

Metal–organic frameworks (MOFs) are porous solids constructed from coordination bonds between organic ligands and metal clusters. These compounds have properties such as large porosity, high surface area, and high thermal/chemical stability, suggesting their potential in various applications. However, recently, MOF as a sacrificial precursor to synthesize nanomaterials by pyrolysis has been developed to expand its applications [22]. UiO-66-NH2(Hf) is a new kind of MOF materials with larger porosity and higher surface area, targeting the synthesis of HfO_2 NPs. In this work, HfO_2 NPs were prepared by simple calcining of UiO-66-NH2(Hf) for imaging characteristics.

The primary objective of this study was to quantitatively assess the imaging properties of HfO_2NPs in comparison to two ordinary CAs, namely iodine and gadolinium. In particular, we sought to determine the CT number and contrast-to-noise ratio (CNR) of HfO_2NPs compared to the two mentioned CAs when used at equivalent concentrations and maximum X-ray energies from 80 to 140 kVp. A head and neck phantom was designed and implemented as a means to establish a quantitative framework for evaluating and demonstrating the performance of HfO_2NPs in CT imaging compared to the conventional iodine and gadolinium CAs.

2 Experimental

2.1 Materials and Instruments

Hafnium chloride ($HfCl_4$), NH_2-BDC ligand, *N, N′*-dimethylformamide (DMF) and other solvents were used without purification and as purchased from commercial sources (Merck, Darmstadt, Germany). The presence of functional groups and types of vibrational frequency present in the HfO_2NPs were confirmed by Fourier transform infrared (FT-IR) spectroscopy (Alpha Bruker Spectrometer). The surface morphology of HfO_2NPs and energy-dispersive X-ray spectroscopy (EDX) were performed on a scanning electron microscope (SEM) (TESCAN MIRA3, Czech Republic).

2.2 Methods

2.2.1 *HfO_2NP synthesis*

UiO-66(Hf)-NH_2 was synthesized following a previously reported procedure with slight modifications [23]. Briefly, a solution of $HfCl_4$ (1.7 g, ~ 5.2 mmol) and NH2-BDC (5.0 mmol) in 50 mL of water and acetic acid (30/20, v/v) was maintained under reflux and continuous magnetic stirring for 24 h. After the reaction was completed, the solid was filtered and purified, dried, and activated as previously mentioned for the UiO66-(Hf). The solid was then calcined at 550 °C for 4 h. After HfO_2NP synthesis, it was brought to different concentrations of 2.5, 5, and 10 mg/mL, all in the same volume of 15 mL.

2.2.2 Concentration and volume equalization

We conducted a comparative analysis employing commercially accessible contrast media: Visipaque™, which includes 320 mg/ml iodine, and Dotarem (0.5 mmol/mL), comprising gadolinium. To assist in standardizing the concentrations of HfO_2NP solutions, the formula $C_1V_1 = C_2V_2$ was implemented, where 'C' and 'V' denote concentration and volume, respectively. Initially, the requisite volume was calculated for each concentration and distilled water was added to reach a volume of 15 mL.

2.2.3 Phantom designing

A polyethylene cylindrical phantom was meticulously fabricated, with dimensions of 200 mm in diameter and 100 mm in height. To facilitate the evaluation of three distinct CAs, nine hollow polyethylene cylindrical tubes with a height of 5 cm, a thickness of 5 mm, and an internal radius of 10 mm were precisely embedded around the central axis to securely accommodate the samples. The center of each tube was situated at a consistent distance of 45 mm from the phantom's edge, ensuring uniformity in the experimental setup. Imaging phantom tubes were also prepared from solutions of gadolinium, iodine, HfO_2NPs, water, cork (lung equivalent) and K_2HPO_4 (bone equivalent) to compare with each other.

2.2.4 X-ray CT scanner Image analysis

Imaging of samples was executed using a GE Bright Speed 16 slice CT scanner, manufactured by General Electric Medical Systems (Waukesha, Wisconsin). Evaluations were conducted under the scan conditions of 80–140 kVps, 300 mAs, and a slice thickness of 2.5 mm. In preparation for scanning, the phantom and tubes were filled with water and defined concentrations of the CAs, respectively, and shaken well to ensure a homogeneously dispersed solution before scanning.

2.2.5 Image quantitative assessment

Image analysis was conducted utilizing the embedded software within the CT scanner, and the CT numbers (Hounsfield unit [HU]) were extracted from all images as well as their corresponding standard deviations (SD). A total of 40 slices were acquired for each exposure technique, and from this set, the slice was chosen to exhibit the most pronounced visual image contrast. Within each sample, a 100 mm^2 region of interest (ROI) positioned at the center of each sample was utilized to extract mean HUs. According to the software, both the average and SD of HU were determined for each ROI, and the image contrast was defined as the difference between the HUs of a studied CA and the background (water-filled phantom). The assessment encompassed the evaluation of both contrast-to-noise ratio (CNR) and signal-to-noise ratio (SNR) across all kVp and concentrations employed in this study. The HUs were extracted from each sample by employing ROIs for the CNR and SNR calculations. The CNR and SNR were quantified by the following formulas [24]:

$$\mathrm{CNR} = \frac{(A - B)}{SD},$$

$$\mathrm{SNR} = \frac{\mathrm{mean(HU)}}{\mathrm{SD}}(in the same ROI),$$

where for the CNR formula, the nominator is the ROI value of CAs in each sample (A) minus the ROI value of the water-filled phantom (B), and the denominator is the noise in the image or the SD of the water-filled phantom. Calculating the SNR value for CA images involved dividing the ROI value in the CA by the SD of the same ROI.

2.3 Statistical analysis

All measurements were conducted in triplicate and data are expressed as mean values ± SD (standard deviation). The one-way analysis of variance (ANOVA) followed by Tukey's test as a post hoc at 95% confidence level was used to evaluate the significance of the experimental data using the SPSS software (version 16). A value of $P < 0.05$ was considered to be statistically significant.

3 Results

The SEM equipped with an energy-dispersive X-ray system was used for the characterization of chemical composition and morphology of the samples. The resulting HfO_2NPs were observed by SEM to be ~ 10 nm spheres (Fig. 1).

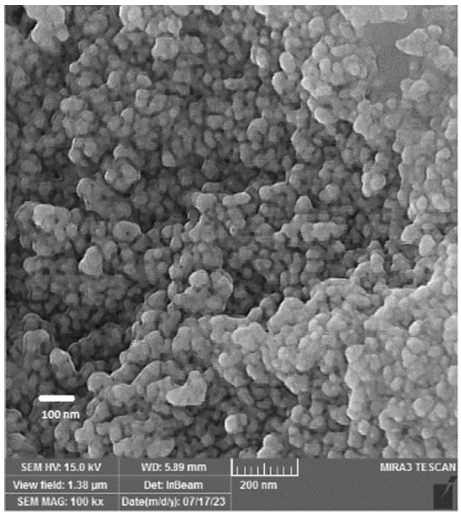

Fig. 1 SEM images of HfO_2NPs

Further characterization of the HfO_2NPs using EDX displayed the presence of Hf and O species in the target material, which confirmed the successful syntheses (Fig. 2). FT-IR spectrum of the prepared nanomaterial was obtained in the range 400–4000 cm^{-1}. As given in Fig. 3, the characteristic strong bands at 760 and 526 cm^{-1} corresponded to Hf–O in the crystalline hafnium oxide. The absorption bands at 3452 and 1629 cm^{-1} are related to the H–O–H stretching modes and bending vibration of the free or physically adsorbed water, respectively. These results are in good agreement with the already reported IR data [25].

Figure 4a shows the 2D grayscale CT image slice of (clockwise from top) 5 mg/ml gadolinium, 5 mg/ml iodine, 5 mg/ml HfO_2NPs, K_2HPO_4 20% (spongiosa equivalent chemical composition), cork (lung equivalent), 2.5 mg/ml HfO_2NPs, 2.5 mg/ml iodine, 2.5 mg/ml gadolinium, and water at the center. The exposure technique was 140 kVp and 300 mAs. In Fig. 4b, the results utilized to elucidate the impact of increased kVp on the HU of the studied CAs for 5 mg/ml concentration. Evidently, Fig. 5 demonstrates that, for all concentrations, HfO_2NPs consistently delivered higher CT numbers compared to iodine and gadolinium at energies higher than 100 kVp. Notably, the HU of the HfO_2NPs, in the case of 5 mg/ml compared to other CAs, improved the visibility and detectability of the tube significantly. Comprehensive results of HU measurements for all CA studies were obtained. At a concentration of 10 mg/ml, the highest HU obtained for the CAs tubes were 194.3 ± 4.21, 178 ± 7.5, and 210.1 ± 8.24 for HfO_2NPs, iodine, and gadolinium at 100, 80, and 80 kVp, respectively. Notably, the rate of HU reduction with increasing beam energy was not uniform across all CAs. The case of a concentration of 10 mg/mL and varying kVp from 80 to 140 led to decreasing the HU of 10%, 87.9%, and 43.2% for HfO_2NPs, iodine and gadolinium, respectively. Based on the statistical analysis conducted, it was found that with the exception of the comparison between gadolinium (Gd) and hafnium (Hf), contrast agents at 2.5 mg/ml concentration under 80 kVp, and the comparison between iodine (I) and Hf contrast agents at 5 mg/ml concentration under 80 kVp, there existed statistically significant differences in Hounsfield units (HUs) between different contrast agents across all kilovoltage and concentration settings. This indicates that, for the majority of comparisons, the selection of contrast agent significantly influenced the measured HUs,

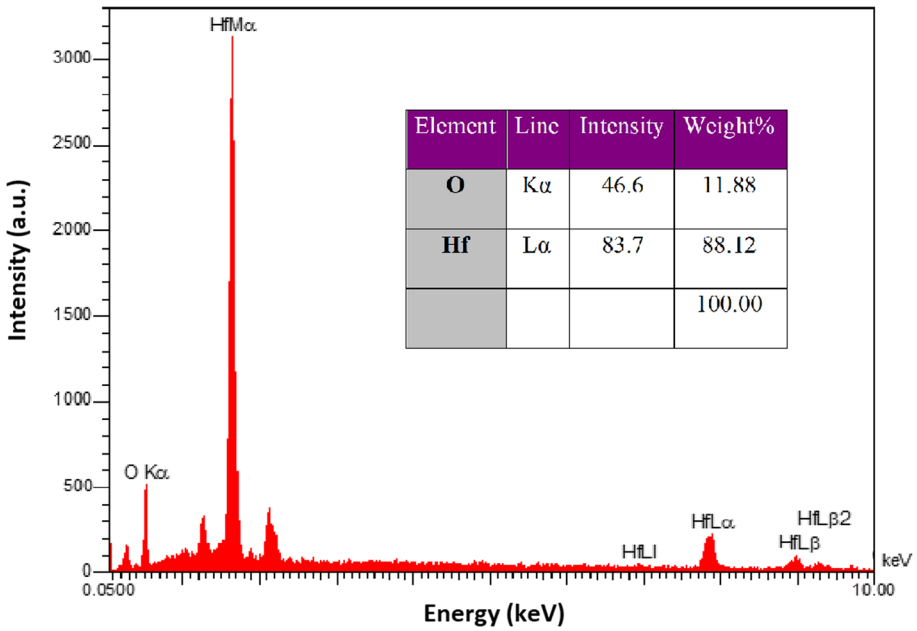

Fig. 2 Experimental EDX patterns and table report of HfO_2NPs

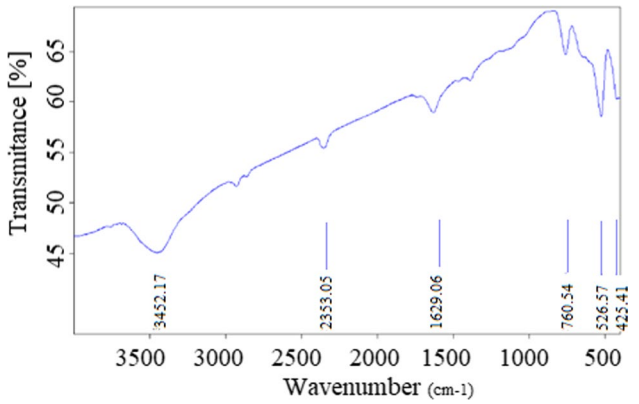

Fig. 3 FT- IR spectrum of HfO_2NPs

underscoring the importance of contrast agent choice in radiological imaging contexts.

It is worth noting that throughout all energies and tube concentrations, the HU of gadolinium-containing tubes exceeded that of iodine tubes. The variation in HU for HfO_2NPs, iodine, and gadolinium is depicted across a photon energy range of 80 to 140 kVp while maintaining a constant mAs of 300. With increasing mean photon energy, HfO_2NPs consistently exhibited higher HU compared to iodine and gadolinium. Furthermore, the HU exhibited a linear decrease with increasing kVp for all CAs and concentrations at the energy ranges above 100 kVp. The peak HU for iodine and gadolinium was observed at 80 kVp, while for HfO2NPs, it reached its maximum at 100 kVp. Particularly, at 2.5 mg/ml concentration and 140 kVp, the HU of HfO_2NPs was 2.3 and 1.3 times greater than that of iodine and gadolinium, respectively. Likewise, within a given concentration and higher kVps, the HU of HfO_2NPs surpassed that of gadolinium, and the HU of gadolinium surpassed iodine.

To illustrate, at the concentration of 2.5 mg/ml and 140 kVp, the CNR of HfO_2NPs exceeded that of iodine by 114% and that of gadolinium by 30%. As shown in Fig. 6, the variation of CNR and SNR with kVp for different concentrations highlights that the CNR and SNR of CAs increased with the concentration for all kVps. As depicted in Fig. 6, instances where the differences are statistically significant are denoted by an asterisk (*). The findings emphasize that under a given concentration and tube potentials above 100 kVp, the CNR of HfO_2NPs consistently surpassed that of iodine and gadolinium. At 80 kVp, gadolinium shows better CNR at all concentrations. Additionally, the CNR of gadolinium exceeded that of iodine across all energies and concentrations. The change in kVp from 80 to 140 and a concentration of 5 mg/mL of CAs resulted in a remarkable increase in CNR for tubes containing HfO_2NPs (101%), iodine (11%), and gadolinium (3%), respectively. Further analysis

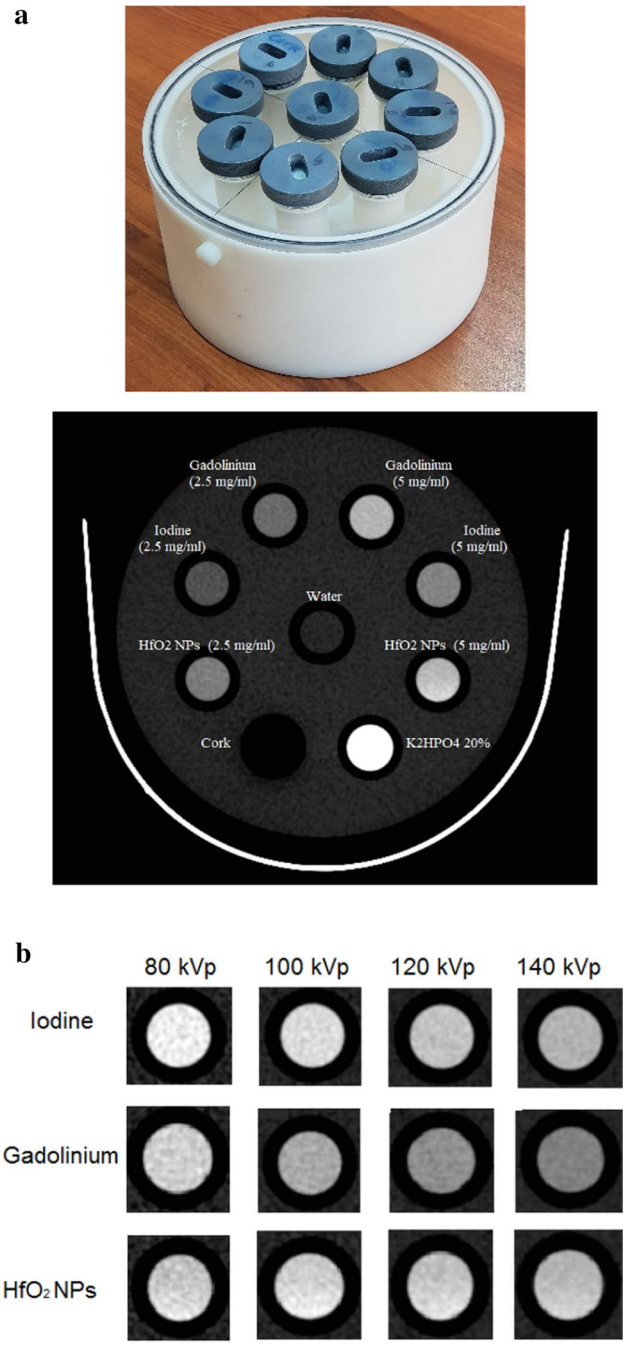

Fig. 4 CT phantom photograph and cross-sectional image of (from the top, counterclockwise) 5 mg/ml gadolinium, 5 mg/ml iodine, 5 mg/ml HfO_2NPs, K_2HPO_4 20% (spongiosa equivalent chemical composition), cork (lung equivalent), 2.5 mg/ml HfO_2NPs, 2.5 mg/ml iodine, 2.5 mg/ml gadolinium, and water at the center (**a**), and CAs at various tube potentials and 300 mAs with concentration of 5 mg/mL (**b**)

focusing on the effect of concentration on CNR revealed notable trends. Under a constant kVp of 140, changing the concentration from 2.5 mg/mL to 10 mg/mL led to a CNR increase of 171%, 229%, and 208.5% for HfO_2NPs, iodine,

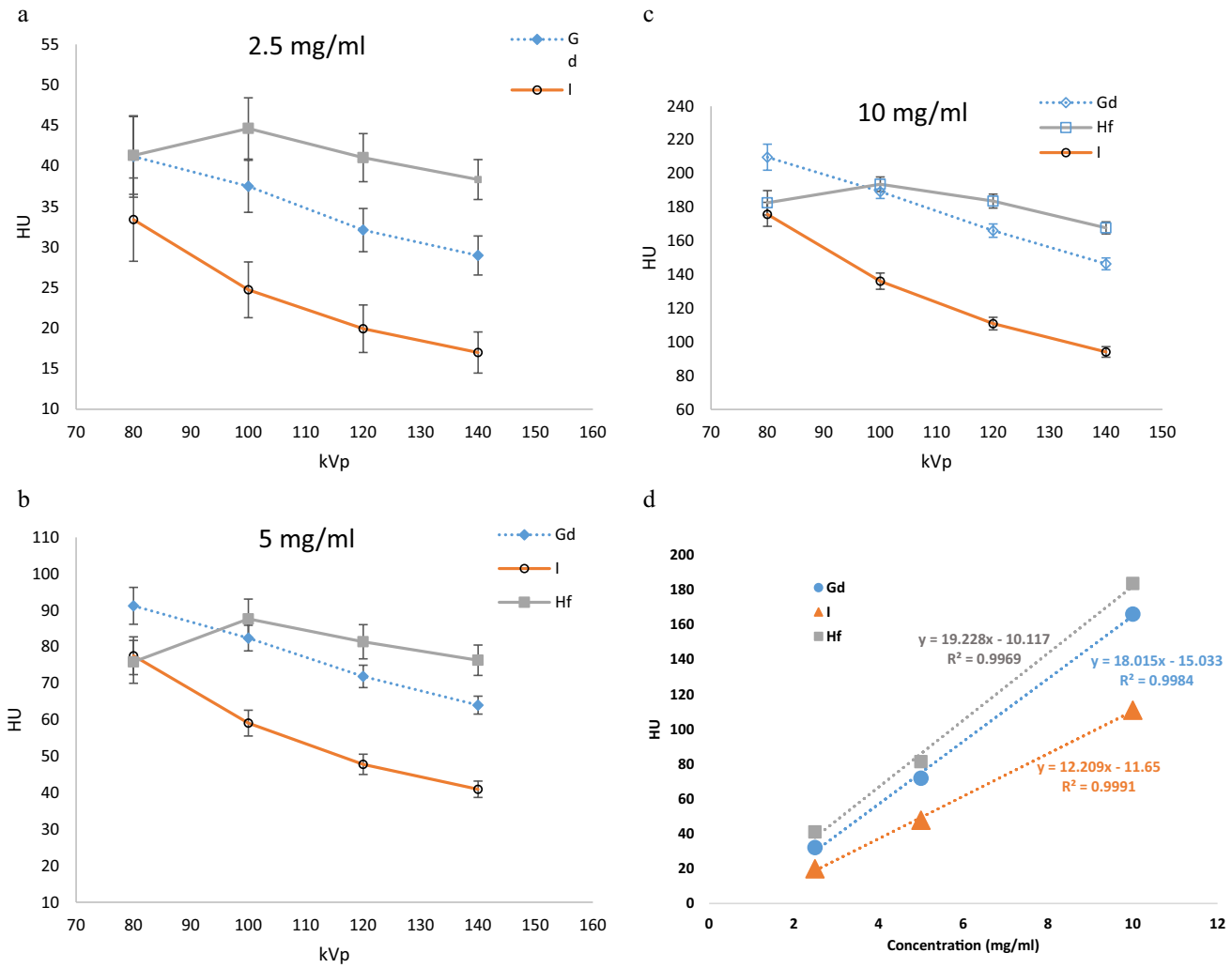

Fig. 5 Comparison of CT number variation of the studied contrast media with beam energy from 80 to 140 kVp and constant mAs = 300 for different concentrations: (**a**) 2.5 mg/ml, (**b**) 5 mg/ml, and 10 mg/ml. (**d**) CT media as a function of concentrations at 120 kVp

and gadolinium, respectively. The supreme CNR were observed at the highest concentration (10 mg/ml) of CAs and 120 kVp. Furthermore, at a concentration of 10 mg/mL of CAs and 140 kVp, the following CNRs were determined for HfO_2NPs, iodine, and gadolinium: 49.6, 28.3, and 43.5, respectively.

4 Discussion

This study presented the imaging characteristics of synthetic HfO_2NPs compared to two traditional CAs. Furthermore, the effects of altering the X-ray tube voltage and different CA concentrations were investigated across constant tube current in CT. The findings demonstrated that, under consistent concentration in tube potential higher energies used in CT scan, HfO_2NPs consistently exhibited significantly higher HUs than both iodine and gadolinium. This higher HU and greater attenuation can be attributed to the higher atomic number and density of Hf ($Z = 72$, density = 13.30 g/cm3) when contrasted with iodine ($Z = 53$, density = 4.93 g/cm^3) and gadolinium ($Z = 64$, density = 7.90 g/cm^3). Basic radiation physics elucidates that photon–matter interactions, primarily governed by photoelectric phenomena, are heavily contingent on atomic number (Z3) in the diagnostic radiology energy range. Similarly, due to gadolinium's elevated atomic number and density compared to iodine, as demonstrated in "Results", gadolinium exhibited superior HU and CNR. This also can be attributed to the photon energy-dependent attenuation coefficients of these elements, as depicted in Fig. 7. Within the photon energy spectra utilized in this study, the peak photon intensity is situated between approximately 50–70 keV.

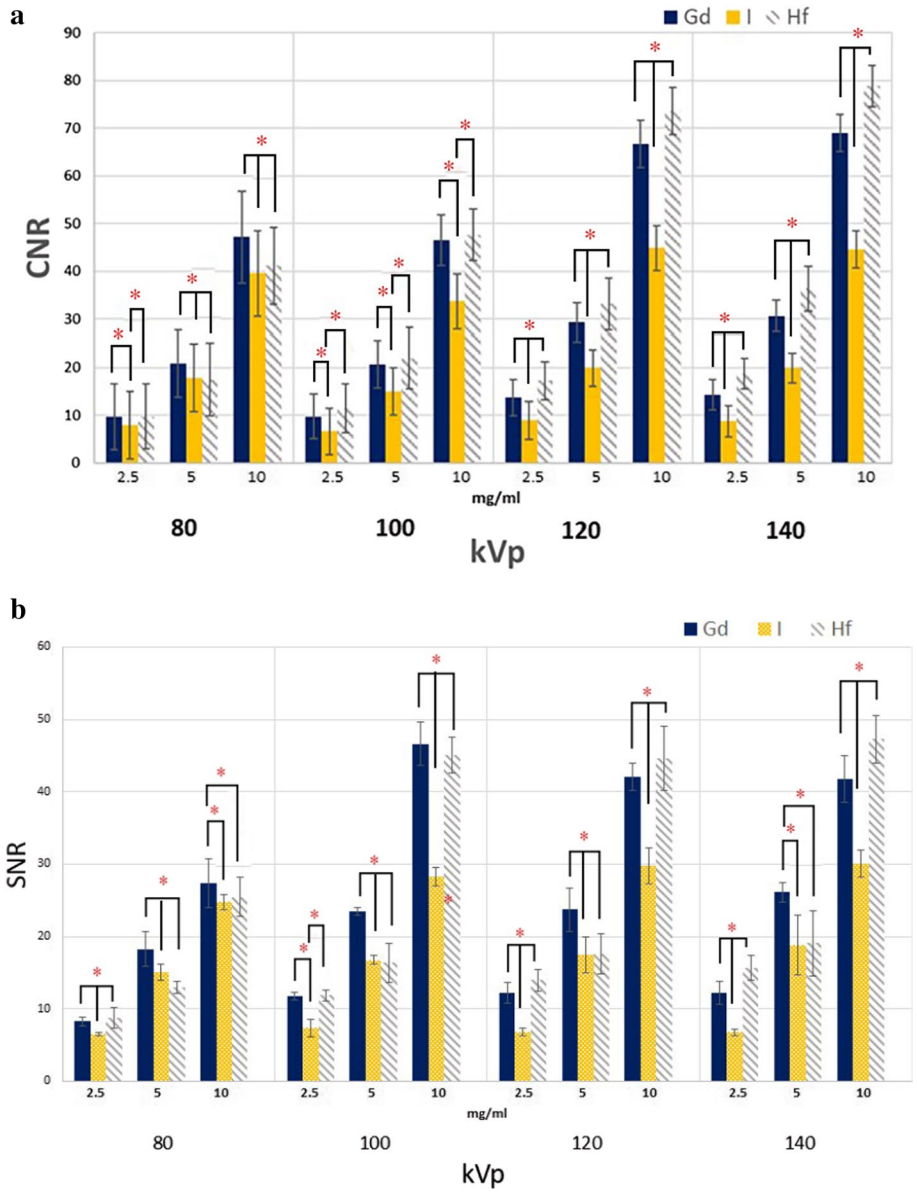

Fig. 6 The CNR (**a**) and SNR (**b**) variations with different kVps and constant mAs of 300 for 2.5, 5, and 10 mg/ml concentration. (*): significant differences

Notably, hafnium, iodine, and gadolinium exhibit K-edge absorption at photon energies of 65.35, 33.2 and 50.2 keV, respectively. Consequently, within the 50–70 keV energy range, hafnium's attenuation outpaces that of iodine and gadolinium, leading to a higher HU for HfO_2NPs in contrast to other two conventional CAs. Aligning with prior research, our results concur with those of Dekrafft et al. and Roessler et al. [26, 27], revealing HU augmentation with increasing CA concentration. The findings further underscore that elevated CA concentration correlates with enhanced image quality in terms of CNR. Increased concentration corresponds to an increased particle count within a defined volume, subsequently increasing the photon–matter interaction and therefore increasing the linear attenuation coefficient and resulting in increased CT number. Moreover, CNRs for all CAs were augmented by higher concentrations and X-ray tube potentials.

When the X-ray tube potential is increased, the energy of the emitted photons is higher. This can reduce the number of photons that are attenuated as they pass through the body, leading to a lower attenuation coefficient. The attenuation coefficient is a measure of how easily the X-ray photons are absorbed by the tissue. A lower attenuation coefficient means that more photons reach the detector, which can result in a lower number of HU across CAs [28]. The Hounsfield unit is a quantitative scale for describing radiodensity in CT imaging, where water is defined as 0 HU and air is defined as -1000 HU. Contrast agents are used to enhance the contrast of structures or fluids within the body in medical imaging. The HU values across these agents can be affected by the

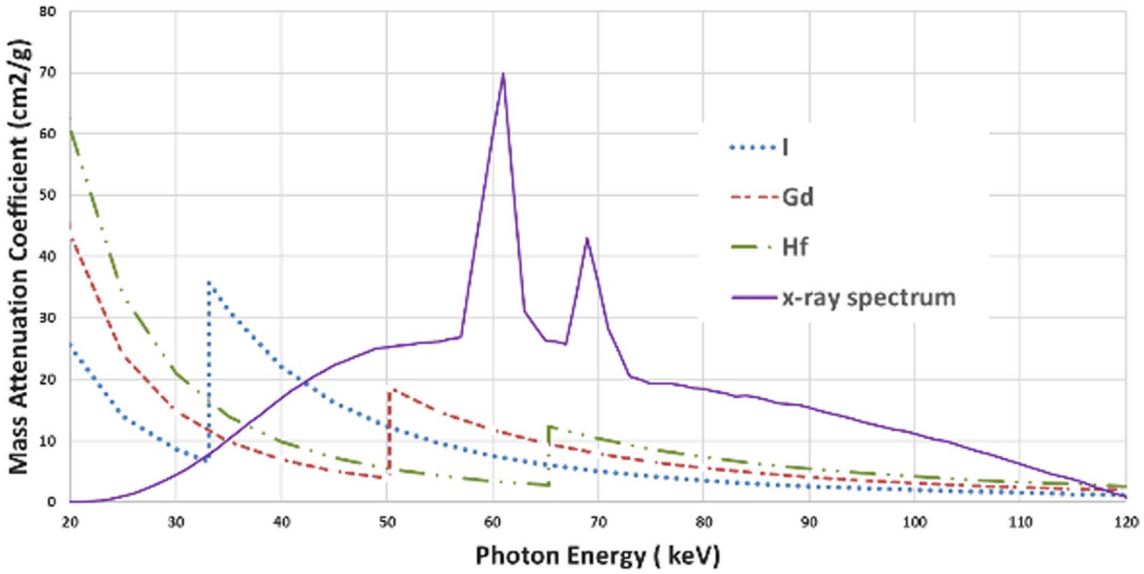

Fig. 7 Mass attenuation coefficient versus photon energy for three elements: Hf, Gd, and I. Theoretical values of the total mass attenuation coefficients were calculated using WinXCom (36)

X-ray tube potential. On the other hand, image noise in CT is primarily quantum noise, which is related to the number of photons that are detected. A higher photon count means that the statistical variation in the number of detected photons (quantum noise) is lower, which reduces the overall image noise. Reduced noise can lead to an increase in the CNR, which is a measure of the contrast of a feature in the image relative to the background noise. A higher CNR means that the feature is more distinguishable from the background, which is generally desirable in medical imaging [29, 30]. In summary, increased X-ray tube potential can lead to a reduced count of attenuated photons and lower HU across contrast agents. Simultaneously, if the overall photon count reaching the detector is higher, this can contribute to reduced image noise and a higher CNR, improving the quality of the CT image. A balance between the energy of the photons (which affects attenuation and HU) and the total number of photons that reach the detector (which affects noise and CNR) is reached [28, 31].

The findings of CNR results compared to analogous studies showed congruence with the results of Su Ya et al., and Nowak et al. [32, 33], indicating that HfO_2NPs, gadolinium, and iodine exhibit increased CNR with escalating CA concentration. In addition, HfO_2NPs demonstrated superior CNR compared to iodine and gadolinium at equivalent concentrations and higher kVps. Iodine contrast media demonstrated superiority in CNR value for tube voltage of 80 kVp, but not higher voltages. The difference between the obtained CNR values of this study and other similar studies may be attributed to the different imaging characteristics of CT scanners, including beam spectra, filtration, detector performance, as well as variations in the CA concentration and synthesis characteristics of the studied particles [16, 34, 35].

5 Conclusion

Enhanced imaging characteristics like contrast-to-noise ratio (CNR) attributes of the HfO_2NPs-derived from UiO-66-NH2(Hf) as a novel contrast agent (CA) revealed in this study, surpassing those of conventional CAs. The results confirmed and integrated into prior research the influence of CA type, concentration, and X-ray tube voltage on both computed tomography (CT) number (HU) and CNR for all three CAs. Remarkably, a consistent trend emerged with HfO_2NPs exhibiting notably superior contrast and enhanced CNR when compared to iodine and gadolinium at higher energies among all concentrations. The topmost HUs were produced at the concentration of 10 mg/ml and 100 kVp settings, while the peak CNR was observed at 120 kVp. As an outcome of this study, we affirm that Hf-based contrast media, specifically in the nanoparticle configuration, delivered substantially heightened contrast levels up to 2.12 times compared to conventional iodine-based CAs, dependent upon tube voltage and concentration. Consequently, using such Hf-based nanoparticles in X-ray CT applications can significantly enhance image quality, thus contributing to improved diagnostic outcomes.

5.1 Disclosures

No conflicts of interest, financial or otherwise, are declared by the authors.

Acknowledgements We wish to thank L. Sanipour, a CT scan technologist at Shiraz's Ali Asghar hospital, who kindly assisted us in acquiring CT images.

Data availability All data in support of the findings of this paper are available within the article.

References

1. De La Vega JC, Häfeli UO. Utilization of nanoparticles as x-ray contrast agents for diagnostic imaging applications. Contrast Media Mol Imaging. 2015;10(2):81–95.
2. Soler L, Delingette H, Malandain G, Montagnat J, Ayache N, Koehl C, et al. Fully automatic anatomical, pathological, and functional segmentation from CT scans for hepatic surgery. Comput Aided Surg. 2001;6(3):131–42.
3. Sharma B, Panta O, Lohani B, Khanal U. Computed tomography in the evaluation of pathological lesions of paranasal sinuses. J Nepal Health Res Counc. 2015;13(30):116–20.
4. Bonnin A, Duvauchelle P, Kaftandjian V, Ponard P. Concept of effective atomic number and effective mass density in dual-energy x-ray computed tomography. Nucl Instrum Methods Phys Res, Sect B. 2014;318:223–31.
5. Vrbaški S, Arana Pena LM, Brombal L, Donato S, Taibi A, Contillo A, et al. Characterization of breast tissues in density and effective atomic number basis via spectral x-ray computed tomography. Phys Med Biol. 2023;68(14):145019.
6. Amato C, Klein L, Wehrse E, Rotkopf LT, Sawall S, Maier J, et al. Potential of contrast agents based on high-z elements for contrast-enhanced photon-counting computed tomography. Med Phys. 2020;47(12):6179–90.
7. Sugawara H, Suzuki S, Katada Y, Ishikawa T, Fukui R, Yamamoto Y, et al. Comparison of full-iodine conventional CT and half-iodine virtual monochromatic imaging: advantages and disadvantages. Eur Radiol. 2019;29:1400–7.
8. Cormode DP, Skajaa T, Van Schooneveld MM, Koole R, Jarzyna P, Lobatto ME, et al. Nanocrystal core high-density lipoproteins: a multimodality contrast agent platform. Nano Lett. 2008;8(11):3715–23.
9. Haller C, Hizoh I. The cytotoxicity of iodinated radiocontrast agents on renal cells in vitro. Invest Radiol. 2004;39(3):149–54.
10. Nazıroğlu M, Yoldaş N, Uzgur EN, Kayan M. Role of contrast media on oxidative stress, Ca 2+ signaling and apoptosis in kidney. J Membr Biol. 2013;246:91–100.
11. Uca YO, Hallmann D, Hesse B, Seim C, Stolzenburg N, Pietsch H, et al. Microdistribution of magnetic resonance imaging contrast agents in atherosclerotic plaques determined by LA-ICP-MS and SR-μXRF imaging. Mol Imag Biol. 2021;23:382–93.
12. Perelli F, Turrini I, Giorgi MG, Renda I, Vidiri A, Straface G, et al. Contrast agents during pregnancy: pros and cons when really needed. Int J Environ Res Public Health. 2022;19(24):16699.
13. Bhave G, Lewis JB, Chang SS. Association of gadolinium based magnetic resonance imaging contrast agents and nephrogenic systemic fibrosis. J Urol. 2008;180(3):830–5.
14. Nadjiri J, Pfeiffer D, Straeter AS, Noël PB, Fingerle A, Eckstein H-H, et al. Spectral computed tomography angiography with a gadolinium-based contrast agent. J Thorac Imaging. 2018;33(4):246–53.
15. Lusic H, Grinstaff MW. X-ray-computed tomography contrast agents. Chem Rev. 2013;113(3):1641–66.
16. FitzGerald PF, Colborn RE, Edic PM, Lambert JW, Torres AS, Bonitatibus PJ Jr, et al. CT image contrast of high-Z elements: phantom imaging studies and clinical implications. Radiology. 2016;278(3):723–33.
17. Berger M, Bauser M, Frenzel T, Hilger CS, Jost G, Lauria S, et al. Hafnium-based contrast agents for X-ray computed tomography. Inorg Chem. 2017;56(10):5757–61.
18. Holmes DR. Corrosion of hafnium and hafnium alloys. In: Cramer SD, Covino BS, Jr., editors. Corrosion: materials, vol 13B. ASM International; 2005.
19. Zhang C-B, Li W-D, Zhang P, Wang B-T. First-principles calculations of phase transition, elasticity, phonon spectra, and thermodynamic properties for hafnium. Comput Mater Sci. 2019;157:121–31.
20. Bonvalot S, Rutkowski P, Thariat J, Carrere S, Sunyach M-P, Saada E, et al. A phase II/III trial of hafnium oxide nanoparticles activated by radiotherapy in the treatment of locally advance soft tissue sarcoma of the extremity and trunk wall. Ann Oncol. 2018;29:viii753.
21. Jost G, McDermott M, Gutjahr R, Nowak T, Schmidt B, Pietsch H. New contrast media for K-edge imaging with photon-counting detector CT. Invest Radiol. 2023;58(7):515–22.
22. Daliran S, Oveisi AR, Peng Y, López-Magano A, Khajeh M, Mas-Ballesté R, et al. Metal–organic framework (MOF)-, covalent-organic framework (COF)-, and porous-organic polymers (POP)-catalyzed selective C-H bond activation and functionalization reactions. Chem Soc Rev. 2022;51(18):7810–82.
23. Hu Z, Peng Y, Kang Z, Qian Y, Zhao D. A modulated hydrothermal (MHT) approach for the facile synthesis of UiO-66-type MOFs. Inorg Chem. 2015;54(10):4862–8.
24. Bushong SC. Radiologic science for technologists e-book: radiologic science for technologists e-book. Elsevier Health Sciences; 2020.
25. Murugasamy J, Ramalakshmi N, Pandiyan R, Ayyaru S, Jayaraman V, Ahn Y-H. Synthesis and characterization of sulfonated hafnium oxide nanoparticles for energy storage devices. Inorg Chem Commun. 2022;141: 109615.
26. Dekrafft KE, Boyle WS, Burk LM, Zhou OZ, Lin W. Zr- and Hf-based nanoscale metal–organic frameworks as contrast agents for computed tomography. J Mater Chem. 2012;22(35):18139–44.
27. Roessler A-C, Hupfer M, Kolditz D, Jost G, Pietsch H, Kalender WA. High atomic number contrast media offer potential for radiation dose reduction in contrast-enhanced computed tomography. Invest Radiol. 2016;51(4):249–54.
28. Flohr T, Petersilka M, Henning A, Ulzheimer S, Ferda J, Schmidt B. Photon-counting CT review. Physica Med. 2020;79:126–36.
29. Ibrahim M, Parmar H, Christodoulou E, Mukherji S. Raise the bar and lower the dose: current and future strategies for radiation dose reduction in head and neck imaging. Am J Neuroradiol. 2014;35(4):619–24.
30. Ferrero A, Gutjahr R, Halaweish AF, Leng S, McCollough CH. Characterization of urinary stone composition by use of whole-body, photon-counting detector CT. Acad Radiol. 2018;25(10):1270–6.
31. Long Y, Fessler JA. Multi-material decomposition using statistical image reconstruction for spectral CT. IEEE Trans Med Imaging. 2014;33(8):1614–26.
32. Nowak T, Hupfer M, Brauweiler R, Eisa F, Kalender WA. Potential of high-Z contrast agents in clinical contrast-enhanced computed tomography. Med Phys. 2011;38(12):6469–82.

33. Su Y, Liu S, Guan Y, Xie Z, Zheng M, Jing X. Renal clearable Hafnium-doped carbon dots for CT/Fluorescence imaging of orthotopic liver cancer. Biomaterials. 2020;255: 120110.
34. Mesbahi A, Famouri F, Ahar MJ, Ghaffari MO, Ghavami SM. A study on the imaging characteristics of gold nanoparticles as a contrast agent in x-ray computed tomography. Polish Journal of Medical Physics and Engineering. 2017;23(1):9.
35. McGinnity TL, Dominguez O, Curtis TE, Nallathamby PD, Hoffman AJ, Roeder RK. Hafnia (HfO 2) nanoparticles as an x-ray contrast agent and mid-infrared biosensor. Nanoscale. 2016;8(28):13627–37.
36. Gerward L, Guilbert N, Jensen KB, Levring H. x-ray absorption in matter. Reengineering XCOM Radiat Phys Chem. 2001;60(1–2):23–4.